HHS Public Access

Author manuscript

Circ Res. Author manuscript; available in PMC 2021 October 23.

Published in final edited form as:

Circ Res. 2020 October 23; 127(10): 1288–1305. doi:10.1161/CIRCRESAHA.120.317439.

Shaping Waves of Bone Morphogenetic Protein Inhibition During Vascular Growth

Pierre J. Guihard[1], **Yina Guo**[1], **Xiuju Wu**[1], **Lily Zhang**[1], **Jiayi Yao**[1], **Medet Jumabay**[1], **Yucheng Yao**[1,2], **Alan Garfinkel**[1], **Kristina I. Boström**[1,3]

[1]Division of Cardiology, David Geffen School of Medicine at UCLA, Los Angeles, CA 90095

[2]UCLA Jonsson Comprehensive Cancer Center

[3]Molecular Biology Institute, UCLA

Abstract

Rationale: The bone morphogenetic proteins (BMPs) are essential morphogens in angiogenesis and vascular development. Disruption of BMP signaling can trigger cardiovascular disease such as arteriovenous malformations.

Objective: A computational model predicted that BMP4 and BMP9 and their inhibitors matrix Gla protein (MGP) and Crossveinless-2 (CV2) would form a regulatory system consisting of negative feedback loops with time delays, and that BMP9 would trigger oscillatory expression of the two inhibitors. The goal was to investigate this regulatory system in endothelial differentiation and vascular growth.

Methods and Results: Oscillations in the expression of MGP and CV2 were detected in endothelial cells (ECs) *in vitro*, using qPCR and immunoblotting. These organized temporally downstream BMP-related activities including expression of stalk cell markers and cell proliferation, consistent with an integral role of BMP9 in vessel maturation. *In vivo*, the inhibitors were located in distinct zones in relation to the front of the expanding retinal network, as determined by immunofluorescence. Time-dependent changes of the CV2 location in the retina, and the existence of an endothelial population with signs of oscillatory MGP expression in developing vasculature supported the i*n vitro* findings. Loss of MGP or its BMP4-binding capacity disrupted the retinal vasculature, resulting in poorly formed networks, especially in the venous

Address correspondence to: Dr. Kristina I. Boström, Division of Cardiology, David Geffen School of Medicine at UCLA, Box 951679, Los Angeles, CA 90095-1679, Tel: 310-794-4417, kbostrom@mednet.ucla.edu.

AUTHOR CONTRIBUTIONS

P.J.G. conceptualization, methodology, validation, formal analysis, investigation, data curation, writing – original draft, writing – review & editing, visualization

Y.G. conceptualization, methodology, validation, formal analysis, investigation, data curation

L.Z. investigation, data curation

X.W. methodology, validation, formal analysis, investigation, data curation, visualization

J.Y. investigation, formal analysis

M.J. methodology

Y.Y. conceptualization, investigation

A.G. conceptualization, formal analysis, writing – review & editing, visualization, supervision

K.I.B. conceptualization, formal analysis, writing – original draft, writing – review & editing, visualization, supervision, project administration, funding acquisition

DECLARATION OF INTERESTS

The authors declare no competing interests.

drainage areas, and arteriovenous malformations as determined by increased cell coverage and functional testing.

Conclusions: Our results suggest a previously unknown mechanism of temporal orchestration of BMP4 and BMP9 activities that utilizes the tandem actions of the extracellular antagonists MGP and CV2. Disruption of this mechanism may contribute to vascular malformations and disease.

Graphical Abstract

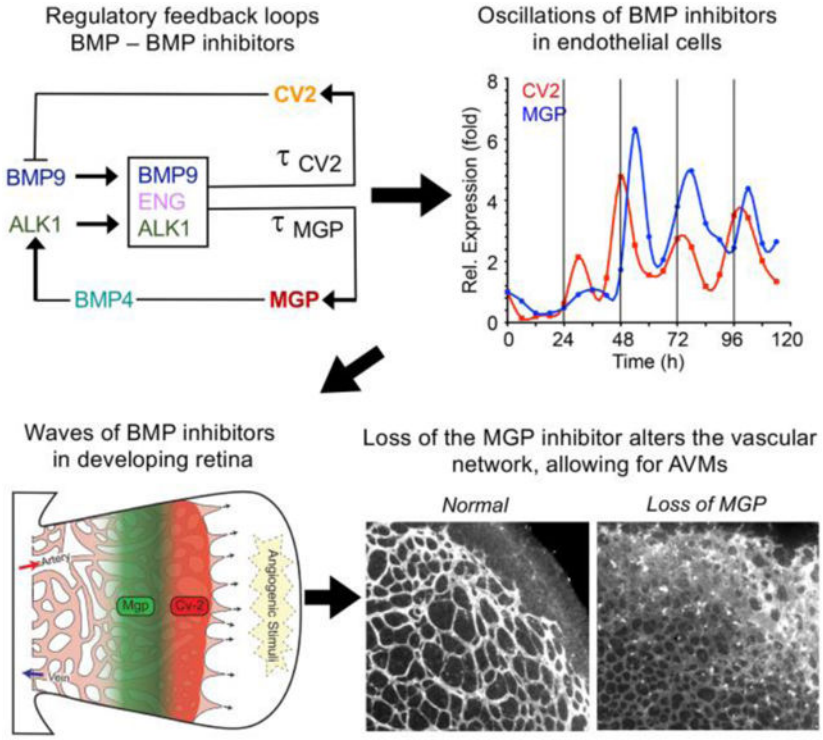

Keywords

Bone morphogenetic protein (BMP); BMP antagonist; matrix Gla protein; crossveinless-2; endothelial cells; angiogenesis; growth factor; Angiogenesis; Basic Science Research; Growth Factors/Cytokines; Vascular Biology

INTRODUCTION

Vascular morphogenesis is essential in development, organogenesis, wound healing [1–3], and vascular disease [1, 4]. The bone morphogenetic proteins (BMPs) participate in tissue patterning during embryogenesis [5–7]. Disruption in BMP signaling during vascular morphogenesis may trigger cardiovascular disease and malformations such as hereditary hemorrhagic telangiectasia (HHT) [4, 8, 9], which is defined by telangiectasia and arteriovenous malformations (AVMs) [10], supporting the idea that genetic defects interfere in the morphogenetic process.

BMP4 and BMP9 are central in vascular formation. BMP4 is expressed locally in tissue and has been described as a pro-angiogenic factor in endothelial cells (ECs) with effects on

proliferation and migration through induction of VEGF and VEGF receptors [11–16]. This is consistent with an early role of BMP4 in the formation of vascular network and endothelial differentiation. BMP9, on the other hand, is secreted from the liver, circulates in the plasma and signals through activin receptor-like kinase (ALK)1 [17, 18]. BMP9 is generally supported as a factor that promotes EC maturation and quiescence (reviewed in [19]) and is known to regulate expression of Notch components and inhibitors of BMPs [20–22]. In previous studies, we demonstrated that BMP4 and BMP9 are linked through ALK1 in ECs. BMP4 induces ALK1 expression through stimulation of the ALK2 receptor [23]. In turn, BMP9 binds to ALK1 and induces two BMP inhibitors, matrix Gla protein (MGP) and Crossveinless-2 (CV2) [15, 21, 23, 24]. CV2 preferentially binds BMP9 with higher affinity than BMP4 [21], whereas MGP binds and inhibits BMP-2, −4, and −7 but not BMP9 [15, 25, 26].

The two inhibitors MGP and CV2 play key roles in vascular morphogenesis. Global gene deletion of *Mgp* in mice causes extensive AVMs throughout multiple organs [15, 27]. Global deletion of the *Cv2* gene in mice, on the other hand, results in thickened endothelium and abnormal expression of endothelial markers in multiple vascular beds [21]. It is not clear if the CV2 deficiency also causes AVMs since complete CV2-deficiency is perinatally lethal due to tracheal abnormalities [28, 29]. Previous studies suggested MGP and CV2 to be essential components of two negative feedback loops, the first loop consisting of ALK1/BMP9 and CV2, and the second loop consisting of BMP4, ALK1/BMP9 and MGP [21]. It is known that negative feedback loops can generate oscillatory gene expression if there are time delays in the induction of the inhibitors [30, 31]. Important examples of oscillatory genes include p53 [32] and the Notch signaling protein Hes1 [33]. The oscillations serve a critical functional role in creating “shaping waves” [5] that coordinate physiological processes, enabling a “temporal compartmentalization” of processes that need to be sequential or are incompatible [34]. In angiogenesis a regulatory loop between BMP/TGFβ-Smad1/5 and Notch signaling orchestrates tip- versus stalk-cell selection under the control of genes that oscillate with opposite phases [5, 35]. During embryogenesis, oscillatory gene expression involving Notch signaling, a target of BMP, is critical for somitogenesis [33, 36, 37]. This is known as the “segmentation clock”, where rhythmic production of somites forms a periodic spatial pattern [36].

Here we identify a novel mechanism of temporal orchestration that is generated by combining the negative feedback loops of BMP4/MGP and BMP9/CV2, using ALK1 as a central node in the system. Our results suggest that during vascular formation, EC maturation is permitted by the integration of waves of extracellular BMP inhibitors in response to BMP9/ALK1/Endoglin signaling. Thus, a lack or mutation of one of these molecular partners, as in HHT or MGP deficiency, will disrupt expression of MGP and CV2 and result in abnormal vascular patterning.

METHODS

The authors declare that all supporting data are available within the article (and its online supplementary files). The code for the computational model is freely available upon request.

Computational model.

Our computational model is a double-loop negative feedback system. Our previous results suggest that BMP4 and BMP9 signaling is organized through two feedback loops [21] with BMP4/MGP and BMP9/CV2 as two agonist-antagonist pairs, and BMP9 as a triggering factor for MGP and CV2 induction.

The key features of our model are:

1. BMP9 is secreted from the liver and circulates in active form in the blood stream [17]. When BMP9 binds to the receptor ALK1 in the presence of coreceptor Endoglin, this BMP9-Endoglin-ALK1 trio induces the expression of CV2 and MGP with time delays τ_{CV2} and τ_{MGP}, respectively.
2. CV2 inhibits BMP9's ability to bind with ALK1, so CV2 acts as an inhibitor of BMP9 [21].
3. BMP9 induces Endoglin activity, which then induces the BMP9-Endoglin-ALK1 trio binding's activities [38].
4. MGP inhibits BMP4 activities [26].
5. BMP4 autocatalytically induces itself in a nonlinear manner, with saturation [39, 40].
6. BMP4 activates ALK1 activity by inducing the expression of the ALK1 receptor (through binding with the ALK2 receptor [23]). There is a time delay τ_{ALK1} in this process.

These effects are summarized in a six variable differential equation, expressing the interactions among the key species:

$$BMP9: \frac{dA}{dt} = k_A - \theta_{AC} AC - \mu_A A$$

$$BMP4: \frac{dB}{dt} = \frac{k_B B^2}{q^2 + B^2} - \theta_{BM} BM - \mu_B B$$

$$ENG: \frac{dE}{dt} = \frac{k_E A^2}{p^2 + A^2} - \mu_E E$$

$$ALK1: \frac{dS}{dt} = k_S B(t - \tau_{ALK1})^2 - \mu_S S$$

$$MGP: \frac{dM}{dt} = k_M A(t - \tau_{MGP}) S(t - \tau_{MGP}) E(t - \tau_{MGP}) - \theta_{BM} BM - \mu_M M$$

$$CV2: \frac{dC}{dt} = k_C A(t-\tau_{CV2}) s(t-\tau_{CV2}) E(t-\tau_{CV2}) - \theta_{AC} AC - \mu_C C$$

In the BMP9 equation, the variable A denotes the concentration of BMP9 (ng/ml). BMP9 is present in the human plasma at a concentration of 2–12 ng/ml [17]. In the model, BMP9 is constantly being supplied at a rate k_A; in the simulations in this paper, we set $k_A = 0$, because BMP9 was not being continuously supplied. Instead, BMP9 was given a large initial concentration. CV2 inhibits BMP9 by binding to it. This inhibitory effect is modeled as a multiplicative negative term in the BMP9 concentration A and the CV2 concentration C with a binding rate θ_{AC}, yielding the term θ_{AC}AC. BMP9 is also removed from the system by degradation at a rate μ_A (hr^{-1}).

In the BMP4 equation, the variable B denotes the concentration of BMP4 (ng/ml). BMP4 is regulated by an autocatalytic process with saturation, which is modeled by a sigmoidal function

$$\frac{k_B B^2}{1 + q^2 B^2}$$

The parameter k_B ($ng \cdot ml^{-1} \cdot hr^{-1}$) represents the maximum production rate of BMP4 by autocatalysis. The parameter q ($ng \cdot ml^{-1}$) is the concentration of BMP4 which gives rise to half of its maximum production rate. MGP inhibits BMP4 through protein-protein interactions [26]. This direct binding is represented by a multiplicative term θ_{BM}BM, which is the product of the concentration of BMP4, B, and the concentration of MGP, M, with a binding coefficient θ_{BM}, representing the binding efficiency of BMP4 and MGP. BMP4 is also degraded, at a rate μ_B.

In the Endoglin equation, the variable E denotes the concentration of Endoglin (ng/ml). Endoglin's production is activated by BMP9 with saturation. Therefore, Endoglin's production rate is a function of the BMP9 concentration. We model this activation-with-saturation process by a sigmoidal term

$$\frac{k_E A^2}{p^2 + A^2}$$

The parameter k_E ($ng \cdot ml^{-1} \cdot hr^{-1}$) is the maximum production rate, while parameter p ($ng \cdot ml^{-1}$) is the concentration of BMP9 at which the Endoglin production is half of its maximum production rate. Endoglin is also decaying at a rate μ_E (hr^{-1}).

In the ALK1 equation, the variable S denotes the concentration of ALK1 (ng/ml). ALK2 is the preferred membrane bound receptor for BMP4, and BMP4 signaling through this receptor is the driving factor for ALK1 expression.

When BMP9 binds to ALK1 in the presence of Endoglin, this trio-complex induces the production of MGP and CV2. *These activation processes occur with considerable time*

delays. For MGP, we use τ_{MGP} to denotes the time delay that it takes for the trio-complex to activate MGP production. For CV2, we use τ_{CV2} to denote the time delay. When the trio binding happens, it activates MGP and CV2 with different efficiencies, k_M and k_C, respectively. The trio-complex is represented as $k_M A(t-\tau_{MGP})\circ S(t-\tau_{MGP})\circ E(t-\tau_{MGP})$ and $k_C A(t-\tau_{CV2})\circ S(t-\tau_{CV2})\circ E(t-\tau_{CV2})$ in the MGP and CV2 equations.

The code was written and executed in Mathematica although given the code, it could be easily run on other software platforms. The code is freely available upon request.

Parameter estimations.

The behavior of a model like ours is dependent on the values of the many parameters in it. Therefore, we carried out experiments to determine the approximate values of as many of these as possible. We were particularly concerned to establish approximate values for the delay constants, τ_{MGP}, τ_{CV2}, and τ_{ALK1}. The experiments establishing these parameter estimations are described fully in the Supplemental Methods.

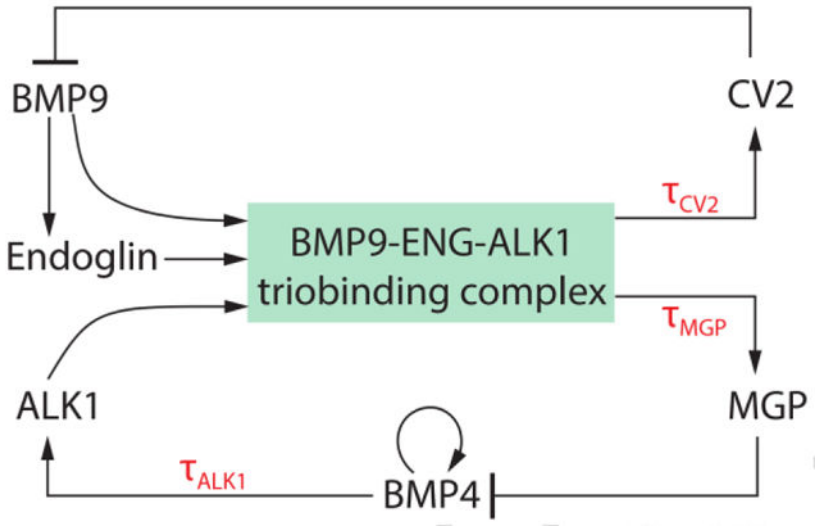

Computational Model - Parameter Values—Parameters and their estimated values in the double-loop mathematical model.

Parameters	Value	Units	Description
k_A	0.3	$ng \cdot ml^{-1} \cdot hr^{-1}$	BMP9 production rate
k_B	0.2	$ng \cdot ml^{-1} \cdot hr^{-1}$	BMP4 maximum production rate
k_E	4	$ng \cdot ml^{-1} \cdot hr^{-1}$	Endoglin maximum production rate
k_S	1	$ng \cdot ml^{-1} \cdot hr^{-1}$	ALK1 production rate
k_M	2	$ng^{-2} \cdot ml^{2} \cdot hr^{-1}$	MGP production rate
k_C	2	$ng^{-2} \cdot ml^{2} \cdot hr^{-1}$	CV2 production rate
θ_{AC}	0.5	$ng^{-1} \cdot ml \cdot hr^{-1}$	Binding rate of BMP9 and CV2
θ_{BM}	0.1	$ng^{-1} \cdot ml \cdot hr^{-1}$	Binding rate of BMP4 and MGP

Parameters	Value	Units	Description
μ_A	0.5	hr^{-1}	Degradation rate of BMP9
μ_B	0.1	hr^{-1}	Degradation rate of BMP4
μ_E	0.5	hr^{-1}	Degradation rate of Engdolin
μ_S	1.5	hr^{-1}	Degradation rate of ALK
μ_M	0.7	hr^{-1}	Degradation rate of MGP
μ_C	0.7	hr^{-1}	Degradation rate of CV2
p	$\sqrt{0.1} \approx 0.31$	$ng \cdot ml^{-1}$	
q	$\sqrt{2} \approx 1.4$	$ng \cdot ml^{-1}$	
τ_{MGP}	2	hr	MGP transcriptional time delay
τ_{CV2}	8	hr	CV2 transcriptional time delay
τ_{ALK1}	1	hr	ALK1 transcriptional time delay

We assume the initial conditions are:

Chemicals	Initial condition
BMP9	$A_0 = 1 ng/ml$
BMP4	$B_0 = 1 ng/ml$
MGP	$M_0 = 1 ng/ml$
CV2	$C_0 = 1 ng/ml$
ALK1	$S_0 = 1 ng/ml$
Endoglin	$E_0 = 1 ng/ml$

Mice.

Mgp$^{+/-}$ (*Mgp*-KO) mice [15, 41], *Bmp4*$^{+/-}$ mice [42] and wild type mice, all on C57BL/6J background, were obtained from the Jackson Laboratory. *Please see the* Major Resource Table *in the* Supplemental Materials. The generation of the *Mgp*$^{mut/mut}$ (*Mgp*-knockin, *Mgp*-KI) mouse is outlined in the Supplemental Material. Genotypes were confirmed by PCR [21], and experiments were performed with generations F4-F6. Littermates were used as wild type controls. All mice were fed a standard chow diet (Teklad Rodent Diet 8604, Envigo, Placentia, CA). The pulmonary vasculature was visualized by micro CT imaging with 3-D reconstructions as previously described [15]. The use of animals and all experimental procedures were reviewed and approved by the University of California Los Angeles (UCLA) Chancellor's Animal Research Committee and conducted in accordance with the animal care guideline set by UCLA. The investigation conformed to the National Research Council, *Guide for the Care and Use of Laboratory Animals, Eighth Edition* (Washington, DC: The National Academies Press, 2011).

Male and female mice were analyzed together since the vascular phenotype in MGP-deficiency is 100% penetrant and we were unable to detect gender differences between male and female mice. No mice were excluded from the analyses.

Time course experiments.

For time course experiments, ECs were plated in 12-well tissue culture plates at a confluence of 80–85% (40K cells/well, 10.5K cells/cm^2) or 50–55% (25K cells/well, 6.5K cells/cm^2). The cells were treated at the time of plating with BMP9 (10 ng/ml, R&D Systems) unless otherwise specified. Oscillation occurred as early as 12 hours after plating at high density and 48 hours after plating at low density. All media were tested to be free of BMP9 prior to the addition of the exogenous BMP9 by ELISA (R&D Systems). BMP4 (R&D Systems) was used at a concentration of 50 ng/ml for cell treatment unless otherwise specified. We carefully checked for interfering factors but found no influence on the oscillations of the time of day of plating of the cells, adding the BMP9, or collecting the samples. Furthermore, we used different models of incubators and monitored for inappropriate variations in room or incubator temperature, oxygen and CO_2 concentrations without finding causes of false positive oscillations. In addition, no oscillations were detected in GAPDH, beta-actin, or alternate control genes used for normalization, including RNA polymerase II and ribosomal protein S29, which could have caused false results.

See Supplemental Material for additional details on the parameters for the computational model and other experimental procedures.

RESULTS

In the mathematical model, time delays are required for the system to generate oscillatory temporal behavior. The character of these oscillations depends on the particular time delays. To study this phenomenon systematically, we carried out 250,000 simulations, a 500 X 500 sampling of the 2-dimensional phase space spanned by τ_{CV2} and τ_{MGP}. We collected the results of these simulations into a phase diagram (Figure 1A): given a pair of values for τ_{CV2} and τ_{MGP}, the diagram shows when the model predicts oscillatory behavior, and the period of the resulting oscillation, if any. We then conducted experiments to determine the values of τ_{CV2} and τ_{MGP} for a variety of ECs, thereby locating each cell type as a point in the phase diagram. This enabled us to test the model, by generating predictions of how each cell type should behave, (oscillatory or not, and, if oscillatory, with what frequency) based on the two-time delays for that cell type.

The components of the model (as described in the Methods section) include the BMP inhibitors CV2 and MGP, the BMP receptors ALK1, ALK2, and Endoglin, and BMP4. These were expressed at different levels in various ECs as shown in Figure 1B. Primary pulmonary artery ECs (HPAECs) were chosen as the central cell model since AVMs were consistently found in the pulmonary vasculature in our previous studies of *Alk1*$^{+/-}$ and *Mgp* $^{-/-}$ mice [15, 43]. Human aortic ECs (HAECs) of low and high passage (p) ($p<5$ and $p>10$, respectively) were used for comparison. Immortalized human brain ECs (HBECs) and adipose-derived stem cells (referred to as dedifferentiated fat or DFAT cells) were used as models of MGP-deficient ECs and EC progenitor cells, respectively. We found that ECs with low expression of MGP tended to have high expression of CV2 and vice versa. In addition, high MGP and ALK1 levels were associated with high expression of BMP4, whereas expression of ALK2 was similar in the different ECs.

We then determined the induction delays of CV2 (τ_{CV2}) and MGP (τ_{MGP}) in response to BMP9 in the different cells (Online Figure IA). Two types of responses in CV2 and MGP were distinguished. A weak response to BMP9 was found in HBECs and DFAT cells. HBECs, in particular, did not respond to BMP9 by increasing MGP or CV2, and DFAT cells only showed an increase in CV2 (τ_{CV2} ~ 40 hours) but not MGP. In these cases, the model predicted no oscillations in MGP and CV2 expression.

A robust response to BMP9 was seen in HPAECs. τ_{CV2} was approximately 6 hours, while τ_{MGP} was about 42 hours (Online Figure IA), coordinates that were in an area that predicted oscillations in these ECs, with a period of ~25 hours (Figure 1A). We then tested the HAEC-high passage, and found that the τ_{CV2} and τ_{MGP} were approximately 15 and 12 hours, respectively, and were at the boundary of the “no oscillation” area of the phase diagram. Since MGP expression was routinely high in HAEC-high passage (Figure 1B), we also compared to HAECs of low passage (similar to the HPAECs) and with less MGP. Indeed, τ_{CV2} was similar to the HPAECs at approximately 6 hours, while τ_{MGP} was about 30 hours in HAEC-low passage (Online Figure IA). These coordinates were in an area that predicted oscillations with periods of ~25 hours, similar to the HPAECs (Figure 1A). We also tested human saphenous veins ECs (HSVECs), and found τ_{CV2} and τ_{MGP} to be approximately 12 and 18 hours, respectively, which predicted oscillations with a period of approximately 25 hours.

Temporal oscillations of CV2 and MGP in the various cell types.

We then tested the various cell types for evidence of oscillatory expression. We treated HPAECs (40,000 cells/well) with 10 ng/ml of BMP9 for up to 5 days with collection of RNA and protein every 6 or 8 hours. Prior to the treatment, all cells had been grown in BMP9-free medium and the addition of exogenous BMP9 synchronized the cells, which coupled to each other through the surrounding medium.

HBECs and DFAT cells showed no oscillations of CV2 or MGP in response to BMP9 (Figure 1C, top). This is to be expected from the model since neither cell type showed a response in MGP.

The HPAECs, on the other hand, were predicted to oscillate. The initial results showed that the CV2 and MGP transcripts oscillated with a period of approximately 24 hours (Figure 1C, center). This was further confirmed in both q6- and q8-hour collection protocols (Figure 2A). Immunoblotting was consistent with the qPCR results and showed CV2 and MGP proteins as waves with a similar period of 24 hours (Figure 2B). As suggested by the simulations, we found that the CV2 transcript preceded the MGP transcript by approximately 6 hours, best visualized with 6-hour collections (Figure 2A). We carefully checked for potentially interfering factors as described in the Methods sections. We also applied non-linear polynomial regression to the time series and used adjusted R^2, which indicated that the variations in gene expression were consistent with periodic oscillations (see figure legend and Supplemental Methods). Multiple testing was not considered across the many tests performed.

We also performed the same experiments using 25,000 HPAECs/well, with similar but less distinct oscillations (Figure 2C), or replaced the medium with new BMP9-containing medium after 60 hours, which disrupted the oscillations that were dependent on interplay between secreted CV2 and MGP (Figure 2D). Without replacement, the BMP9 gradually declined in the medium over the course of the experiment, as assessed by ELISA, but remained in the physiological range of 2–12 ng/ml [17] for about 100 hours (Online Figure IB). The expression lost its oscillations after about 100–120 hours. None of the ECs used in the study expressed BMP9. The period of the oscillations was similar between experiments even though the amplitudes varied, as shown when the initial two oscillations from nine different experiments were compared (Figure 2E).

Both HAECs-low passage cells and HSVEC resembled the HPAECs in regards to induction delays, and CV2 and MGP expression oscillated with similar periods in both cell types as predicted by the phase diagram (Figure 1C, bottom). The HAECs-high passage, however, responded to BMP9 by increasing CV2 and MGP expression but without distinct oscillations (Figure 1C, bottom), potentially due to the high baseline expression of MGP (Figure 1B). *In summary,* in each cell type, we found that the observed behavior matched the predictions of the phase diagram.

BMP9 triggers stalk cell marker expression in HPAECs.

Vascular growth may proceed through phases or waves of proliferation and differentiation to form the vascular structures. BMP4 is known to affect VEGF expression and proliferation [11–15, 44], whereas most studies have linked BMP9 to stalk cell differentiation [19]. Therefore, we hypothesized that oscillations in stalk cell markers might be induced as BMP9 gains access to the growing vessels through circulating blood. To further investigate the behavior of tip versus stalk cell markers, we validated that the HPAECs expressed stalk cell markers in response to BMP9 but not BMP4 as shown in Online Figure II. We also compared the effects of BMP4 and BMP9 on parameters associated with vascular growth including VEGF expression, cell numbers, and growth patterns in the HPAECs as in Online Figures II and IIIA. BMP4, in particular, induced VEGF and stimulated proliferation.

We established a working model of the angiogenic front incorporating the actions of BMP4 and BMP9 (Figure 3A): BMP4 is available from exogenous sources or local ECs and induces expression of ALK1 and VEGF [15, 45]. ALK1 is then stimulated by circulating BMP9. BMP9 induces CV2 and MGP that antagonize BMP9 and BMP4 and coordinate their actions.

This model predicts that induction of VEGF by BMP4 is an essential link in stimulating vascular outgrowth in organs like the lungs where BMP4 is essential for development [46, 47]. To confirm this, we examined mice heterozygous for *Bmp4* gene deletion (*Bmp4*$^{+/-}$) mice by micro-CT imaging, and found a 25% reduction in vessel surface (p=8.0e-4) and a 50% reduction in vessel volume (p=4.2e-4) as assessed by micro-CT (Figure 3B) indicating the importance of BMP4 in vessel growth.

The model also predicted potential waves or oscillations in downstream stalk cell markers and in proliferation in response to BMP9. Therefore, the tip markers CD34 and Dll4, and the

stalk markers HEY1 and JAG1 were assessed in samples from the time course experiments with BMP9-treated HPAECs. Indeed, we found a similar oscillatory expression pattern for HEY1 and JAG1, whereas the expression of CD34 and Dll4 declined rapidly over the first 24 hours (Figure 3C). Application of non-linear regression to the time series and adjusted R^2 indicated that the variations in gene expression were consistent with periodic oscillations (see figure legend). In several of the periods, the sequence of the peaks of expression was CV2, JAG1, HEY1 and MGP (Figure 3D), suggesting that the inhibitor actions are tightly synchronized. Oscillations in the stalk marker expression were also detected in the HAEC-low passage cells, but not in the HBECs that lacked inhibitor oscillations (Figure 1C).

Our computational model also predicted oscillations in the BMP4 and Endoglin expression. We were able to detect these as relatively low amplitude oscillations in many of the experiments (Online Figure IIIB), although they were often below reliable detection.

We next examined how MGP expression related to cell proliferation in HPAECs treated with control or BMP9 (10 ng/ml). Samples for CV2 and MGP expression were collected every 6 hours, and proliferation was measured in periods of 6 hours. The results showed that once the inhibitor oscillations were established, the proliferation curve became more periodic in appearance with peaks of proliferation at times when the inhibitor expression was low (Figure 4). Together, the results suggested that the gene expression and proliferation can be coordinated by the BMP inhibitors.

Spatial patterns of CV2 and MGP in retinal angiogenesis.

Temporal oscillations can be used for spatial patterning or organization, provided that the information from the oscillating system can be registered within the tissue so as to leave a permanent repetitive pattern. In somitogenesis, the segmentation of the presomitic mesoderm is regulated be the segmentation clock [48], which is periodic but only exist for the purpose of the one-time patterning of the developing embryo. The segmentation clock has been studied both in isolated presomitic mesoderm cell cultures as well as in the presomitic mesoderm [48, 49].

For the vasculature, we studied the oscillatory system involving CV2 and MGP in cultured ECs. Similar to the segmentation clock, the existence of this system would serve the one-time patterning of a vascular network created using the rise and fall of CV2 and MGP to sweep through the nascent network optimizing cell proliferation and differentiation. The previous finding that vascular morphogenesis is disrupted in the *Mgp*-KO mice, with frequent AVMs [15, 27], may be consistent with lack of oscillations in the absence of MGP (see for example HBEC in Figure 1C).

It is not possible to perform time course experiments or synchronization in specific cells *in vivo*.

Therefore, we first turned to postnatal retinal angiogenesis [50] to investigate if *in vivo* evidence supported our model. We verified that expression of ALK1 and Endoglin, responsible for the BMP9 signaling, was detectable in the postnatal day (P)7 retina from wild type mice as shown in Online Figure IV.

We predicted that CV2 would be found in expanding areas where it would help limit endothelial maturation to allow for growth (Figure 5A for schematic model). Indeed, CV2 stained close to the front especially in the venous collection system (Figure 5B). However, CV2 was not expressed in the tip cells, as shown by the co-staining with Isolectin B4 (Figure 5C) and confocal microscopy (Figure 5D), which supports that CV2 is induced by the initial exposure to blood and circulating BMP9. There was also a gradual decrease of CV2 towards the center of the retina, in a reverse pattern to the distribution of CD31, a marker of mature ECs (Online Figure VA). We confirmed that cell proliferation was higher in the venous collection areas enriched with CV2 by injecting the pups with EdU 2 hours prior to euthanasia and assessing the proliferation by immunostaining for EdU (Online Figure VB).

Next, we examined if the location of CV2 would be time-dependent. We visualized CV2 in retinas from P6 through P9. The results showed that on P6, CV2 was found close to the front and subsequently moved across the retina (Figure 6). On P8 and P9, CV2 staining had largely disappeared as the retina reached full dimensions, except for penetrating new vessels (Figure 6). The results supported a rapid passage or wave of CV2 during network formation.

We then predicted that MGP would be found in in proximity of CV2 but away from the front. Indeed, the highest expression of MGP was located in partly overlapping areas in the plexus (Figure 5B). MGP co-stained with Isolectin B4-positive cells adjacent to the spaces in the vascular structures.

Since MGP tends to be incorporated in matrix [25], we used an alternative approach to test for MGP oscillations in developing networks. We used a publicly available data set of single cell (sc)RNA-sequencing (seq) from developing lungs with time points between embryonic day (E)12.5 and P7 [51]. We identified a sub-population of pulmonary ECs that expressed multiple lineage markers, including CD31 and VE-Cadherin (EC cluster 3, Figure 7A). Gene ontology analysis showed that the top markers in the EC3 cluster were classified under EC migration, regulation of Notch signaling, circulatory system development and angiogenesis (Figure 7B). Specifically, the EC3 cluster expressed ALK1, MGP, Hey1, and Jag1 (Figure 7C), which corresponds to that observed in the cultured HPAECs. We then applied a statistical approach to the combined EC3 cluster cells referred to as Oscope for identification of oscillatory gene groups in unsynchronized scRNA seq data sets [52]. Indeed, MGP was identified as an oscillatory gene in the EC3 cluster (Figure 7D). This supports that our cell system had correctly identified *Mgp* as a gene with oscillatory expression that could serve as a driver of morphogenic cycles.

Effect of MGP deficiency on retinal angiogenesis - changes that can lead to AVMs.

MGP deficiency *in vivo* leads to AVMs in lungs, kidneys and brain [15, 27]. Low MGP expression *in vitro* was associated with absence of oscillations and high CV2 in the HBECs and DFAT cells (Figure 1A, C). Our previous results from aorta also showed that absence of MGP enhanced CV2 expression and proliferation in aorta [21]. Thus, we speculated that the retina would also be abnormal in MGP-deficiency, with high CV2 expression and AVMs.

To test this, we prepared retinas from *Mgp*-knockout (KO) and *Mgp*-knockin (KI) mice, where *Mgp* had been mutated and lost the ability to bind and inhibit BMP4 (see Methods).

We hypothesized that the *Mgp*-KI mice would show similar changes to the *Mgp*-KO mice presuming that the changes were driven by lack of BMP antagonism. The retinas from P7 wild type, *Mgp*-KO and *Mgp*-KI mice were stained with Isolectin B4 to assess the vascular networks. The *Mgp*-KO and *Mgp*-KI retinas were highly vascular, especially in the venous collection system (Figure 8A) where the cell coverage increased about 1.5-fold (p=1.0e-4) compared to wild type (Figure 8B), which would allow for formation of AMVs. In addition, the venous (V) diameter tended to be larger than the arterial (A) diameter in the *Mgp*-KO and *Mgp*-KI retinas (Figure 8A, B).

Retinas from P7 wildtype and *Mgp*-KO mice were then stained with anti-CV2 antibodies, which showed increased CV2 in the *Mgp*-KO retinas, especially in the retinal vein (V) and the plexus that it drained (Figure 8C). This supports that CV2 has a role in limiting BMP9 activity to allow expansion. Finally, we examined the distribution of alpha-smooth muscle actin (ASMA) in the three types of retina to assess for changes in arterial identity in the networks. As expected, ASMA was found mainly in the retinal artery in wild type mouse (Figure 8D, left panels). However, in both the *Mgp*-KO and the *Mgp*-KI retinas, ASMA was visible also in the veins (Figure 8D, middle and right panels). In the *Mgp*-KO retinas in particular, ASMA was detected in vessels that drained into the large veins (Figure 8D, middle panels). The results suggested that abnormal AV-connections result from the abnormal networks and may explain the ubiquitous AVMs in lungs, kidneys and brain previously reported in the *Mgp*-KO mice [15, 27]. To confirm the presence of AVMs, we performed functional assays by injecting fluorescent microspheres and determining whether these were retained in the retina. As expected, the microspheres were retained in the normal retinas but not in the AVMs in the *Mgp*-KO retinas, with a near 100% reduction in retained microspheres (p=1.6e-2) (Online Figure VI).

DISCUSSION

We have identified a novel mechanism of temporal orchestration in vascular growth, generated by the tandem actions of the two BMP inhibitors MGP and CV2. Our results suggest that EC differentiation and vascular formation are dynamically regulated by temporal waves of these BMP inhibitors, expressed in response to BMP9 signaling. These have the ability of modulating the activities of BMP4 and BMP9 to rise and fall as required for an alternating sequence of proliferation and differentiation.

Mechanism of Oscillation.

Physiological oscillations often have as their mechanism the action of negative feedback loops, operating in the presence of time delays [30]. For example, the 2017 Nobel Prize in Physiology or Medicine was awarded for the discovery of the mechanism of the circadian rhythm, in which “several transcription factors operate in a genetic network incorporating autoregulatory [negative] feedback loops. Oscillations are achieved by delaying various steps in the network.” [53]. In our case, the negative feedback relation is created by BMP9 and BMP4 together inducing the production of their inhibitors, MGP and CV2. This is confirmed by our mathematical model, a double-loop negative feedback system including time delays. The model correctly predicts, based on the characteristics of each cell type,

whether that cell type has oscillatory production of CV2 and MGP or not, and with what period.

Functional role of oscillation.

A critical function of oscillation is to reconcile incompatible processes by cycling between them. This was first proposed in an early study of metabolic processes [54]. The authors observed that glycolysis and gluconeogenesis have incompatible requirements, which are reconciled within the cell by oscillation between the two processes, a phenomenon they called “temporal organization” (for a discussion of this point, see also [55])

Another example of the functional role of oscillation can be found in the study of Tu et al. of cyclic processes in yeast metabolism [34]. They found that many genes were expressed rhythmically. Interestingly, the rhythmic behaviors were organized into 3 distinct groups of mutually exclusive processes, cycling each in turn. They called this phenomenon “temporal compartmentalization”.

Angiogenesis.

In EC maturation and angiogenesis, the temporal compartmentalization may occur between proliferation and differentiation. Conditions for alternating waves of proliferation and maturation are created by the induced oscillations in the BMP inhibitors, which provides inhibition for BMP9 and BMP4 and produce oscillations in downstream gene expression. The dual induction of CV2 and MGP provides inhibition for BMP9 and BMP4, respectively. In each cycle, the induction of CV2 occurs first with an edge of about 6 hours and is aimed at BMP9. The induction of MGP follows and is aimed at BMP4. Thus, every cycle generates a shift from BMP9 inhibition (BMP4 dominance) to BMP4 inhibition (BMP9 dominance). BMP4 may act on proliferation and recruitment of early progenitors, whereas BMP9 commits the cells to stalk cell differentiation. The stalk cell markers show an oscillatory pattern that reflects the alterations in BMP9 activity. Thus, the antagonism produced by the waves of CV2 and MGP may lead to i) proliferation or recruitment of early ECs, ii) tip cell inhibition, iii) induction of stalk cell phenotype, iv) formation of lumen and quiescence.

Other mechanisms of BMP oscillations in vascular development.

There have been a number of interesting observations of functional oscillations involving BMPs and their inhibitors in vascular development. In a review of the dynamics of stalk cells and tip cells, Beets et al. [5] spoke of these oscillations as creating “shaping waves”: phases of tip cell favoring conditions alternating with phases of stalk-cell favoring conditions. The mechanism proposed is a negative feedback loop: BMPs induce SMADs, which induce Notch, an inhibitor of BMPs. A similar theme can be found in a series of papers from Bentley’s group [56, 57]. They also locate the mechanism of oscillation in a negative feedback loop involving BMPs and Notch signaling inhibiting BMPs.

However, there are several important differences between their oscillations and ours. First of all, our oscillations are generated in response to a stimulus of BMP9. Second, their negative feedback loop requires Notch and DLL4, whereas we find that DLL4 is suppressed throughout the response to BMP9. Third, importantly, the oscillations that they discuss are

occurring at an ultradian time scale, 2–3 hours, as opposed to ours, which are roughly 24-hour rhythms. Fourth, their oscillations create shaping waves that consist of periods of stalk-cell favoring conditions alternating with periods of tip-cell favoring conditions. Our 24-hr oscillations, which are induced by BMP9 (as opposed to the ultradian oscillations) appear have a distinct mechanism (involving the BMP inhibitors MGP and CV2) as well as a distinct functional role (establishing a cycle between proliferation and differentiation, as opposed to tipness/stalkness).

One study that did use a BMP9 stimulus was a study by Eichmann's group [20]. Their HUVEC cells, when stimulated by BMP9, suppressed tip cell markers (such as DLL4) and increased HEY1 and JAG1. This agrees with our findings. (Their study did not attempt to resolve a time course for this induction). In the oscillation between tip-ness and stalk-ness, they suggest that inhibition of BMP9 is necessary: "In addition, it is possible that BMP antagonists may modulate BMP9 activity in the vasculature, even though BMP9 and BMP10 have not been reported to interact with BMP antagonists noggin or follistatin." Our results suggest that CV2 is another inhibitor of BMP9 that may play a critical role in creating oscillations.

24-hour and circadian rhythms in BMPs.

The rhythms we observed in MGP and CV2 have a period of roughly 24 hours. We emphasize that this period emerges directly from the time delays involved in the induction of the inhibitors CV2 and MGP by BMP4 and BMP9, according to our mathematical model. In the literature, the term "circadian rhythm" is sometimes used to refer to any 24-hour rhythm, and sometimes used more strictly to mean "a rhythm whose mechanism is the cyclic expression of the circadian genes, such as *Clock, Bmal1, Per* and *Tim".* Our rhythms are probably not 'circadian' in the stricter sense. We did not see any significant changes in clock gene expression in our cultures over the course of the experiments (Online Figure VII for *Clock* and *Bmal1*). Neither did we detect any oscillatory behavior in the phosphatase and tensin homolog (PTEN) gene (Online Figure VII), which has been associated with endothelial quiescence [58]. Our rhythms appear to have a mechanism independent of the circadian genes, although it is obvious that since they have a roughly 24-hour period, they are ideally suited to synchronize to the circadian rhythms.

Several studies have discussed circadian rhythms (in the narrow sense) in BMPs. One study focused on the role of Gremlin-2, a known inhibitor of BMP4, that is controlled by the circadian clock, concluding "the circadian clock controls BMP signaling" [59]. Yet other studies have found evidence for a causal relation in the opposite direction: "we show that the Bone Morphogenetic Protein (BMP) signaling pathway plays a crucial role in setting the circadian period" [60]. Of course, both findings can well be correct, suggesting that BMP signaling may be involved in a feedback relation with the circadian gene expression system.

The rhythms we see in the BMP inhibitors appear to be independent of the circadian gene system, and have a 24-hour period that is explained by the negative feedback dynamics of BMP4 and 9 and their inhibitors. How this rhythm synchronizes with, is affected by, and causes changes in the circadian gene system is an interesting question for further research, as

is the question of how our (and other) 24-hour rhythms interact with the 2–3 hour rhythms seen in other studies.

Waves in the retinal vascular network.

Oscillatory behaviors have been described during embryogenesis, indeed it has been shown that temporal gene expression is critical for morphogenetic processes such as somitogenesis, where Notch signaling, a target of BMP pathways, plays a central role [33, 36, 37]. In the retina, CV2 was always detected closest to the angiogenic front, suggesting that CV2 preceded MGP in a manner consistent with the cell experiments. None of the inhibitors were detected in the tip cells that are not exposed to the circulating BMP9.

AVMs.

In the *Mgp*-KO mice, which are known to exhibit abnormal AV connections with full penetrance [15, 27], the increased CV2 level at the front is likely to contribute to the dense vasculature by delaying the EC differentiation. This may also happen in patients with Keutel syndrome, the human analogue to the *Mgp*-KO mouse. However, the only reported visualization of the lung vasculature from such a patient is a limited study demonstrating varicose-like vessels with multiple peripheral artery stenoses [61].

In HHT, which is characterized by partial deficiency of Endoglin and ALK1 and AVMs with variable penetrance [10], disruption of MGP and possibly CV2 expression are likely to contribute to the AVMs. We have shown that $Alk1^{+/-}$ mice have about half the amount of MGP, and about 15% have pulmonary AVMs similar to human patients with HHT [43]. Breeding of the $Alk1^{+/-}$ mice with *Mgp*-transgenic mice fully prevented the AVMs [43]. Interestingly, $Alk1^{+/-}$ cells were predicted to have less pronounced oscillations in our computational model, which might be consistent with the variable penetrance observed in HHT although this was not tested.

Vascular networks bridge the arterial and venous side of the circulation and is frequently the location of AVMs. The mechanism that we have outlined for using inhibitors to organize proliferation and cell differentiation is likely to work for both arterial and venous ECs. Indeed, we see oscillations in the HSVECs (Figure 1C) and the largest changes in the MGP-deficient retinas are in the venous runoff areas (Figure 8). However, the exact inhibitors may differ between ECs depending on the organ location.

Supplementary Material

Refer to Web version on PubMed Central for supplementary material.

ACKNOWLEDGMENTS

Funding for this work was provided in part by NIH/NHLBI: grant number HL30568 (K.I.B.), NIH/NHLBI: grant number HL81397 (K.I.B.), NIH/NINDS: grant number NS79353 (Y.Y.), NIH/NHLBI: grant number HL139675.

Nonstandard Abbreviations and Acronyms:

A	Arterial

ALK	Activin receptor-like kinase
ASMA	Alpha-smooth muscle actin
AVM	Arteriovenous malformation
BMP	Bone morphogenetic protein
CD	Cluster of differentiation (in CD34 and CD31)
CV2	Crossveinless-2
DFAT	Dedifferentiated fat (in DFAT cells)
DLL4	Delta-like ligand 4
EC	Endothelial cell
Gla	Gamma-carboxyglutamic acid
HAEC	Human aortic endothelial cell
HBEC	Human brain endothelial cell
HHT	Hereditary hemorrhagic telangiectasia
HPAEC	Human pulmonary artery endothelial cell
HSVEC	Human saphenous veins endothelial cell
HUVEC	Human umbilical vein endothelial cell
IB4	Isolectin B4
KI	Knockin
KO	Knockout
MGP	Matrix Gla protein
p	passage
P	Postnatal day
qPCR	Quantitative real-time polymerase chain reaction
scRNA seq	Single cell RNA sequencing
V	Venous

REFERENCES

1. Potente M and Makinen T. Vascular heterogeneity and specialization in development and disease. Nature reviews. 2017;18:477–494.
2. Hu K and Olsen BR. The roles of vascular endothelial growth factor in bone repair and regeneration. Bone. 2016;91:30–8. [PubMed: 27353702]

3. DiPietro LA. Angiogenesis and scar formation in healing wounds. Curr Opin Rheumatol. 2013;25:87–91. [PubMed: 23114588]

4. Goumans MJ, Zwijsen A, Ten Dijke P and Bailly S. Bone Morphogenetic Proteins in Vascular Homeostasis and Disease. Cold Spring Harb Perspect Biol. 2018;10.

5. Beets K, Huylebroeck D, Moya IM, Umans L and Zwijsen A. Robustness in angiogenesis: notch and BMP shaping waves. Trends Genet. 2013;29:140–9. [PubMed: 23279848]

6. Bier E and De Robertis EM. EMBRYO DEVELOPMENT. BMP gradients: A paradigm for morphogen-mediated developmental patterning. Science. 2015;348:aaa5838.

7. Raspopovic J, Marcon L, Russo L and Sharpe J. Modeling digits. Digit patterning is controlled by a Bmp-Sox9-Wnt Turing network modulated by morphogen gradients. Science. 2014;345:566–70. [PubMed: 25082703]

8. Morrell NW, Bloch DB, Ten Dijke P, Goumans MJ, Hata A, Smith J, Yu PB and Bloch KD. Targeting BMP signalling in cardiovascular disease and anaemia. Nat Rev Cardiol. 2016;13:106–20. [PubMed: 26461965]

9. Garcia de Vinuesa A, Abdelilah-Seyfried S, Knaus P, Zwijsen A and Bailly S. BMP signaling in vascular biology and dysfunction. Cytokine Growth Factor Rev. 2016;27:65–79. [PubMed: 26823333]

10. Shovlin CL. Hereditary haemorrhagic telangiectasia: pathophysiology, diagnosis and treatment. Blood Rev. 2010;24:203–19. [PubMed: 20870325]

11. Boyd NL, Dhara SK, Rekaya R, Godbey EA, Hasneen K, Rao RR, West FD 3rd, Gerwe BA and Stice SL. BMP4 promotes formation of primitive vascular networks in human embryonic stem cell-derived embryoid bodies. Experimental biology and medicine (Maywood, NJ. 2007;232:833–43.

12. Nimmagadda S, Geetha Loganathan P, Huang R, Scaal M, Schmidt C and Christ B. BMP4 and noggin control embryonic blood vessel formation by antagonistic regulation of VEGFR-2 (Quek1) expression. Dev Biol. 2005;280:100–10. [PubMed: 15766751]

13. Vogt RR, Unda R, Yeh LC, Vidro EK, Lee JC and Tsin AT. Bone morphogenetic protein-4 enhances vascular endothelial growth factor secretion by human retinal pigment epithelial cells. J Cell Biochem. 2006;98:1196–202. [PubMed: 16514669]

14. Goldman O, Feraud O, Boyer-Di Ponio J, Driancourt C, Clay D, Le Bousse-Kerdiles MC, Bennaceur-Griscelli A and Uzan G. A boost of BMP4 accelerates the commitment of human embryonic stem cells to the endothelial lineage. Stem Cells. 2009;27:1750–9. [PubMed: 19544443]

15. Yao Y, Jumabay M, Wang A and Bostrom KI. Matrix Gla protein deficiency causes arteriovenous malformations in mice. J Clin Invest. 2011;121:2993–3004. [PubMed: 21765215]

16. Suzuki Y, Montagne K, Nishihara A, Watabe T and Miyazono K. BMPs promote proliferation and migration of endothelial cells via stimulation of VEGF-A/VEGFR2 and angiopoietin-1/Tie2 signalling. J Biochem. 2008;143:199–206. [PubMed: 18006519]

17. David L, Mallet C, Keramidas M, Lamande N, Gasc JM, Dupuis-Girod S, Plauchu H, Feige JJ and Bailly S. Bone morphogenetic protein-9 is a circulating vascular quiescence factor. Circ Res. 2008;102:914–22. [PubMed: 18309101]

18. Miller AF, Harvey SA, Thies RS and Olson MS. Bone morphogenetic protein-9. An autocrine/paracrine cytokine in the liver. J Biol Chem. 2000;275:17937–45. [PubMed: 10849432]

19. Tillet E and Bailly S. Emerging roles of BMP9 and BMP10 in hereditary hemorrhagic telangiectasia. Front Genet. 2014;5:456. [PubMed: 25620979]

20. Larrivee B, Prahst C, Gordon E, del Toro R, Mathivet T, Duarte A, Simons M and Eichmann A. ALK1 signaling inhibits angiogenesis by cooperating with the Notch pathway. Developmental cell. 2012;22:489–500. [PubMed: 22421041]

21. Yao Y, Jumabay M, Ly A, Radparvar M, Wang AH, Abdmaulen R and Bostrom KI. Crossveinless 2 regulates bone morphogenetic protein 9 in human and mouse vascular endothelium. Blood. 2012;119:5037–47. [PubMed: 22474252]

22. Ricard N, Ciais D, Levet S, Subileau M, Mallet C, Zimmers TA, Lee SJ, Bidart M, Feige JJ and Bailly S. BMP9 and BMP10 are critical for postnatal retinal vascular remodeling. Blood. 2012;119:6162–71. [PubMed: 22566602]

23. Yao Y, Shao ES, Jumabay M, Shahbazian A, Ji S and Bostrom KI. High-density lipoproteins affect endothelial BMP-signaling by modulating expression of the activin-like kinase receptor 1 and 2. Arterioscler Thromb Vasc Biol. 2008;28:2266–74. [PubMed: 18948634]
24. Shao ES, Lin L, Yao Y and Bostrom KI. Expression of vascular endothelial growth factor is coordinately regulated by the activin-like kinase receptors 1 and 5 in endothelial cells. Blood. 2009;114:2197–2206. [PubMed: 19506300]
25. Zebboudj AF, Imura M and Bostrom K. Matrix GLA protein, a regulatory protein for bone morphogenetic protein-2. J Biol Chem. 2002;277:4388–94. [PubMed: 11741887]
26. Yao Y, Shahbazian A and Bostrom KI. Proline and gamma-carboxylated glutamate residues in matrix Gla protein are critical for binding of bone morphogenetic protein-4. Circ Res. 2008;102:1065–74. [PubMed: 18369157]
27. Yao Y, Yao J, Radparvar M, Blazquez-Medela AM, Guihard PJ, Jumabay M and Bostrom KI. Reducing Jagged 1 and 2 levels prevents cerebral arteriovenous malformations in matrix Gla protein deficiency. Proc Natl Acad Sci U S A. 2013;110:19071–6. [PubMed: 24191040]
28. Zakin L, Metzinger CA, Chang EY, Coffinier C and De Robertis EM. Development of the vertebral morphogenetic field in the mouse: interactions between Crossveinless-2 and Twisted Gastrulation. Dev Biol. 2008;323:6–18. [PubMed: 18789316]
29. Ikeya M, Kawada M, Kiyonari H, Sasai N, Nakao K, Furuta Y and Sasai Y. Essential pro-Bmp roles of crossveinless 2 in mouse organogenesis. Development. 2006;133:4463–73. [PubMed: 17035289]
30. Garfinkel A, Shevtsov J and Guo Y. Mechanisms of Oscillation *Modeling Life*: Springer.com; 2017: 172–186.
31. Glass L, Beuter A and Larocque D. Time Delays, Oscillations, and Chaos in Physiological Control-Systems. Math Biosci. 1988;90:111–125.
32. Purvis JE, Karhohs KW, Mock C, Batchelor E, Loewer A and Lahav G. p53 dynamics control cell fate. Science. 2012;336:1440–4. [PubMed: 22700930]
33. Hirata H, Yoshiura S, Ohtsuka T, Bessho Y, Harada T, Yoshikawa K and Kageyama R. Oscillatory expression of the bHLH factor Hes1 regulated by a negative feedback loop. Science. 2002;298:840–3. [PubMed: 12399594]
34. Tu BP, Kudlicki A, Rowicka M and McKnight SL. Logic of the yeast metabolic cycle: temporal compartmentalization of cellular processes. Science. 2005;310:1152–8. [PubMed: 16254148]
35. Moya IM, Umans L, Maas E, Pereira PN, Beets K, Francis A, Sents W, Robertson EJ, Mummery CL, Huylebroeck D and Zwijsen A. Stalk cell phenotype depends on integration of Notch and Smad1/5 signaling cascades. Dev Cell. 2012;22:501–14. [PubMed: 22364862]
36. Hubaud A and Pourquie O. Signalling dynamics in vertebrate segmentation. Nature reviews. 2014;15:709–21.
37. Moreno-Risueno MA, Van Norman JM, Moreno A, Zhang J, Ahnert SE and Benfey PN. Oscillating gene expression determines competence for periodic Arabidopsis root branching. Science. 2010;329:1306–11. [PubMed: 20829477]
38. Scharpfenecker M, van Dinther M, Liu Z, van Bezooijen RL, Zhao Q, Pukac L, Lowik CW and ten Dijke P. BMP-9 signals via ALK1 and inhibits bFGF-induced endothelial cell proliferation and VEGF-stimulated angiogenesis. J Cell Sci. 2007;120:964–72. [PubMed: 17311849]
39. Canalis E, Economides AN and Gazzerro E. Bone morphogenetic proteins, their antagonists, and the skeleton. Endocr Rev. 2003;24:218–35. [PubMed: 12700180]
40. Garfinkel A, Tintut Y, Petrasek D, Bostrom K and Demer LL. Pattern formation by vascular mesenchymal cells. Proc Natl Acad Sci U S A. 2004;101:9247–50. [PubMed: 15197273]
41. Luo G, Ducy P, McKee MD, Pinero GJ, Loyer E, Behringer RR and Karsenty G. Spontaneous calcification of arteries and cartilage in mice lacking matrix GLA protein. Nature. 1997;386:78–81. [PubMed: 9052783]
42. Winnier G, Blessing M, Labosky PA and Hogan BL. Bone morphogenetic protein-4 is required for mesoderm formation and patterning in the mouse. Genes Dev. 1995;9:2105–16. [PubMed: 7657163]

43. Bostrom KI, Guihard P, Blazquez Medela AM, Yao J, Moon JH, Penton A and Yao Y. Matrix Gla protein limits pulmonary arteriovenous malformations in ALK1 deficiency. Eur Respir J. 2015;45:849–52. [PubMed: 25614167]
44. Bai H, Gao Y, Arzigian M, Wojchowski DM, Wu WS and Wang ZZ. BMP4 regulates vascular progenitor development in human embryonic stem cells through a Smad-dependent pathway. J Cell Biochem. 2010;109:363–74. [PubMed: 19950207]
45. Yao Y, Zebboudj AF, Shao E, Perez M and Bostrom K. Regulation of bone morphogenetic protein-4 by matrix GLA protein in vascular endothelial cells involves activin-like kinase receptor 1. J Biol Chem. 2006;281:33921–30. [PubMed: 16950789]
46. Weaver M, Dunn NR and Hogan BL. Bmp4 and Fgf10 play opposing roles during lung bud morphogenesis. Development. 2000;127:2695–704. [PubMed: 10821767]
47. Southwood M, Jeffery TK, Yang X, Upton PD, Hall SM, Atkinson C, Haworth SG, Stewart S, Reynolds PN, Long L, Trembath RC and Morrell NW. Regulation of bone morphogenetic protein signalling in human pulmonary vascular development. J Pathol. 2008;214:85–95. [PubMed: 17992660]
48. Webb AB and Oates AC. Timing by rhythms: Daily clocks and developmental rulers. Dev Growth Differ. 2016;58:43–58. [PubMed: 26542934]
49. Webb AB, Soroldoni D, Oswald A, Schindelin J and Oates AC. Generation of dispersed presomitic mesoderm cell cultures for imaging of the zebrafish segmentation clock in single cells. J Vis Exp. 2014.
50. Tual-Chalot S, Allinson KR, Fruttiger M and Arthur HM. Whole mount immunofluorescent staining of the neonatal mouse retina to investigate angiogenesis in vivo. J Vis Exp. 2013:e50546. [PubMed: 23892721]
51. Cohen M, Giladi A, Gorki AD, Solodkin DG, Zada M, Hladik A, Miklosi A, Salame TM, Halpern KB, David E, Itzkovitz S, Harkany T, Knapp S and Amit I. Lung Single-Cell Signaling Interaction Map Reveals Basophil Role in Macrophage Imprinting. Cell. 2018;175:1031–1044 e18. [PubMed: 30318149]
52. Leng N, Chu LF, Barry C, Li Y, Choi J, Li X, Jiang P, Stewart RM, Thomson JA and Kendziorski C. Oscope identifies oscillatory genes in unsynchronized single-cell RNA-seq experiments. Nat Methods. 2015;12:947–950. [PubMed: 26301841]
53. Young MW and Kay SA. Time zones: a comparative genetics of circadian clocks. Nature reviews. 2001;2:702–15.
54. Boiteux A, Hess B and Sel'kov EE. Creative functions of instability and oscillations in metabolic systems. Curr Top Cell Regul. 1980;17:171–203. [PubMed: 7002485]
55. Garfinkel A A mathematics for physiology. Am J Physiol. 1983;245:R455–66. [PubMed: 6624944]
56. Bentley K, Mariggi G, Gerhardt H and Bates PA. Tipping the balance: robustness of tip cell selection, migration and fusion in angiogenesis. PLoS Comput Biol. 2009;5:e1000549. [PubMed: 19876379]
57. Kur E, Kim J, Tata A, Comin CH, Harrington KI, Costa Lda F, Bentley K and Gu C. Temporal modulation of collective cell behavior controls vascular network topology. eLife. 2016;5.
58. Alsina-Sanchis E, Garcia-Ibanez Y, Figueiredo AM, Riera-Domingo C, Figueras A, Matias-Guiu X, Casanovas O, Botella LM, Pujana MA, Riera-Mestre A, Graupera M and Vinals F. ALK1 Loss Results in Vascular Hyperplasia in Mice and Humans Through PI3K Activation. Arterioscler Thromb Vasc Biol. 2018;38:1216–1229. [PubMed: 29449337]
59. Yeung CY, Gossan N, Lu Y, Hughes A, Hensman JJ, Bayer ML, Kjaer M, Kadler KE and Meng QJ. Gremlin-2 is a BMP antagonist that is regulated by the circadian clock. Sci Rep. 2014;4:5183. [PubMed: 24897937]
60. Beckwith EJ, Gorostiza EA, Berni J, Rezaval C, Perez-Santangelo A, Nadra AD and Ceriani MF. Circadian period integrates network information through activation of the BMP signaling pathway. PLoS Biol. 2013;11:e1001733. [PubMed: 24339749]
61. Parmar H, Blaser S, Unger S, Yoo SJ and Papsin B. Petrified ears in a patient with Keutel syndrome: temporal bone CT findings. Pediatr Radiol. 2006;36:241–3. [PubMed: 16328322]

62. Hartung A, Bitton-Worms K, Rechtman MM, Wenzel V, Boergermann JH, Hassel S, Henis YI and Knaus P. Different routes of bone morphogenic protein (BMP) receptor endocytosis influence BMP signaling. Mol Cell Biol. 2006;26:7791–805. [PubMed: 16923969]

63. Jumabay M, Abdmaulen R, Ly A, Cubberly MR, Shahmirian LJ, Heydarkhan-Hagvall S, Dumesic DA, Yao Y and Bostrom KI. Pluripotent stem cells derived from mouse and human white mature adipocytes. Stem Cells Transl Med. 2014;3:161–71. [PubMed: 24396033]

64. Lee H, Shi W, Tontonoz P, Wang S, Subbanagounder G, Hedrick CC, Hama S, Borromeo C, Evans RM, Berliner JA and Nagy L. Role for peroxisome proliferator-activated receptor alpha in oxidized phospholipid-induced synthesis of monocyte chemotactic protein-1 and interleukin-8 by endothelial cells. Circ Res. 2000;87:516–21. [PubMed: 10988245]

65. Bostrom K, Zebboudj AF, Yao Y, Lin TS and Torres A. Matrix GLA protein stimulates VEGF expression through increased transforming growth factor-beta1 activity in endothelial cells. J Biol Chem. 2004;279:52904–13. [PubMed: 15456771]

66. Yao Y, Bennett BJ, Wang X, Rosenfeld ME, Giachelli C, Lusis AJ and Bostrom KI. Inhibition of bone morphogenetic proteins protects against atherosclerosis and vascular calcification. Circ Res. 2010;107:485–94. [PubMed: 20576934]

67. Bar-Joseph Z Analyzing time series gene expression data. Bioinformatics. 2004;20:2493–503. [PubMed: 15130923]

68. Tian LP, Liu LZ and Wu FX. Nonlinear-model-based analysis methods for time-course gene expression data. ScientificWorldJournal. 2014;2014:313747. [PubMed: 24516364]

NOVELTY AND SIGNIFICANCE

What Is Known?

- Matrix Gla protein (MGP) and Crossveinless-2 (CV2) are inhibitors of bone morphogenetic protein (BMP) 4 and 9, all involved in vascular development.
- Lack of MGP causes arteriovenous malformations (AVMs) in multiple organs.
- A system with two negative feedback loops may give rise to oscillations or waves in gene expression that coordinate cellular actions.

What New Information Does This Article Contribute?

- BMP9-induced expression of MGP and CV2 oscillate in cultured endothelial cells due to feedback regulation, as predicted by a computational model, allowing orchestration of BMP4 and 9 activities.
- In retinal angiogenesis in mice, waves of CV2 and MGP are required for normal development of the vascular network.
- Absence of functioning MGP results in an abnormally dense retinal network that allows the formation of AVMs.

The bone morphogenetic proteins (BMPs) are essential factors in vessel formation. Poor regulation of the BMPs cause vascular disease, including so-called arteriovenous malformations (AVMs). A computer model predicts that two of the BMPs (BMP4 and BMP9) together with their inhibitors matrix Gla protein (MGP) and Crossveinless-2 (CV2) would form a system where BMP9 can trigger oscillations of the inhibitors. We now report that the predicted oscillations are present in cells from vessels. The oscillations help coordinate the required BMP activities. In mouse retinas, the inhibitors are located in distinct zones, with evidence of CV2 and MGP waves. Loss of MGP results in abnormally dense networks of vessels and signs of AVMs. The findings point to a new mechanism of BMP regulation that coordinate cells for the purpose of creating vascular networks thereby avoiding malformations such as AVMs.

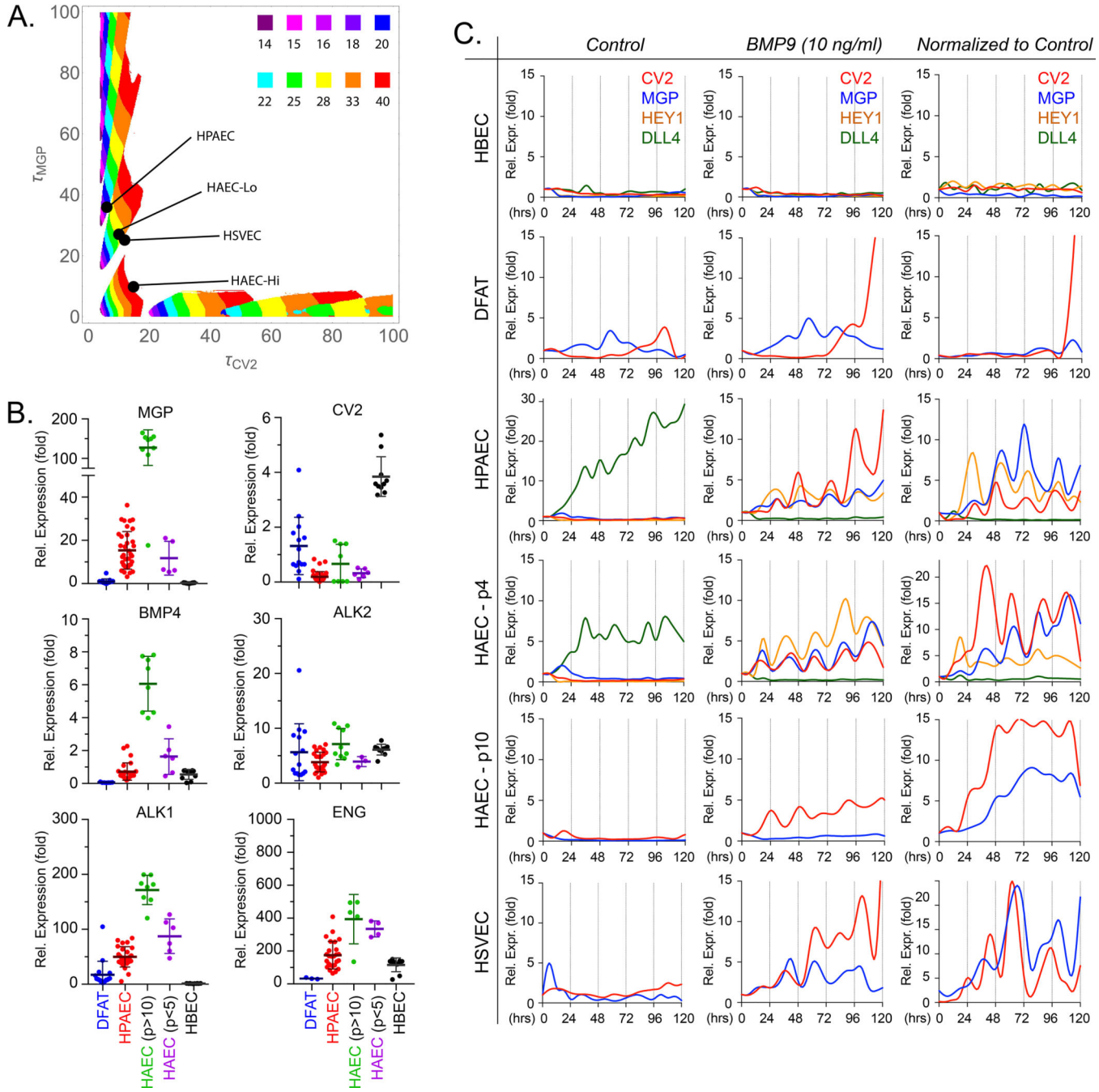

Figure 1: Baseline characteristics of endothelial cells.

(A) *Phase diagram: time delays and the system's temporal behaviors.* The diagram is the result of 250,000 simulations, a 500 X 500 sampling of the 2-dimensional phase space spanned by τ_{CV2} and τ_{MGP}. Given a pair of values for τ_{CV2} and τ_{MGP}, the diagram shows when the model predicts oscillatory behavior, and the period of the resulting oscillation, if any. (B) Baseline expression of MGP, CV2, BMP4, ALK2, ALK1 and ENG in endothelial progenitor cells (DFAT cells) and different preparations of endothelial cells under normal culture conditions, as determined by qPCR. Horizontal bars represent mean ± SD. (C)

Temporal oscillations of CV2 and MGP in different endothelial cells. Expression profiles for CV2 and MGP in HBEC, DFAT cells (EC progenitors), HPAEC, HAEC-passage 10 or HAEC-passage 4 and HSVEC with no treatment (first column), 10 ng/ml of BMP9 (second column). The third column represents BMP9 treatment where each data point has been normalized to its own untreated control. The stalk cell marker HEY1 and the tip cell marker DLL4 are included in the graphs for HBEC, HPAEC, and HAEC-passage 4. RNA was collected every 6 hours for up to 120 hours. Each time point represents the mean of 3 determinations by qPCR, first normalized to GAPDH and then to its own control; 3–8 replicate experiments were performed for each type of EC.
DFAT cells, dedifferentiated cells; EC, endothelial cells; HPAEC, human pulmonary artery EC; HAEC, human aortic EC; HUVEC, human umbilical vein EC; HBEC, human brain EC; HSVEC, human saphenous vein EC; p, passage.

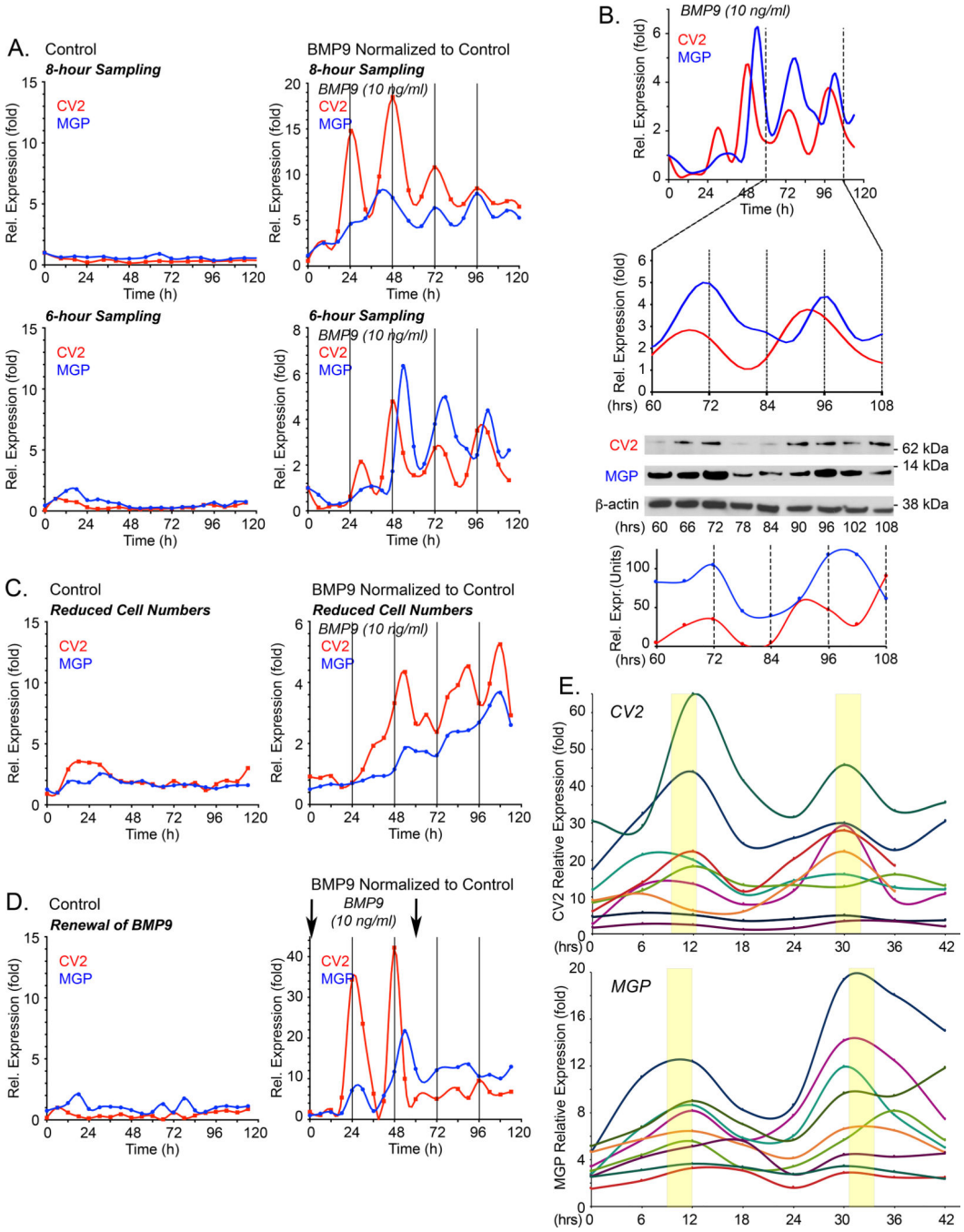

Figure 2: Temporal oscillations of CV2 and MGP transcripts in HPAECs in response to BMP9.

Expression profiles for MGP and CV2 under different conditions. In the following experiments, expression of MGP and CV2 was determined by qPCR, first normalized to GAPDH and then its own control. (A) HPAECs were treated with control medium (left panels) or BMP9 (10 ng/ml) (right panels), RNA was collected every 8 or 6 hours for up to 120 hours, and expression of CV2 and MGP was determined by qPCR. Adjusted R^2 and p-values from non-linear polynomial regression were as follows: *8-hour collection*: *MGP*: adjusted R^2 0.841, p-value 7.63E-05; *CV-2*: adjusted R^2 of 0.674, p-value 0.003; *6-hour*

collection: *MGP*: adjusted R^2 0.499, p-value 0.005; *CV-2*: adjusted R^2 0.406, p-value 0.027. For 8- and 6-hour collections, 3 and 5 replicate experiments were performed, respectively. (B) Corresponding CV2 and MGP protein levels from cells treated with BMP9 (10 ng/ml), between 60–108 hours (qPCR, immunoblot and image quantification) (representative of 3 replicate experiments). (C) HPAECs seeded at low density (6.25×10^3 cells/cm^2), treated with control medium (left panel) or BMP9 (10 ng/ml) (right panel). RNA was collected every 6 hours for up to 120 hours, and expression of CV2 and MGP was determined by qPCR (duplicate experiments). (D) HPAECs were treated with control medium (left panel) or BMP9 (10 ng/ml) added at the time of plating and 60 hours later (arrows) (right panel). RNA was collected every 6 hours for up to 120 hours, and expression of CV2 and MGP was determined by qPCR (duplicate experiments). (E) HPAECs treated with BMP9 (10 ng/ml) for 42 hours; two early oscillations from 9 replicate experiment are shown.
Each qPCR time point represents the mean of 3 determinations, and each BMP9-treated time point is normalized to its own untreated control.

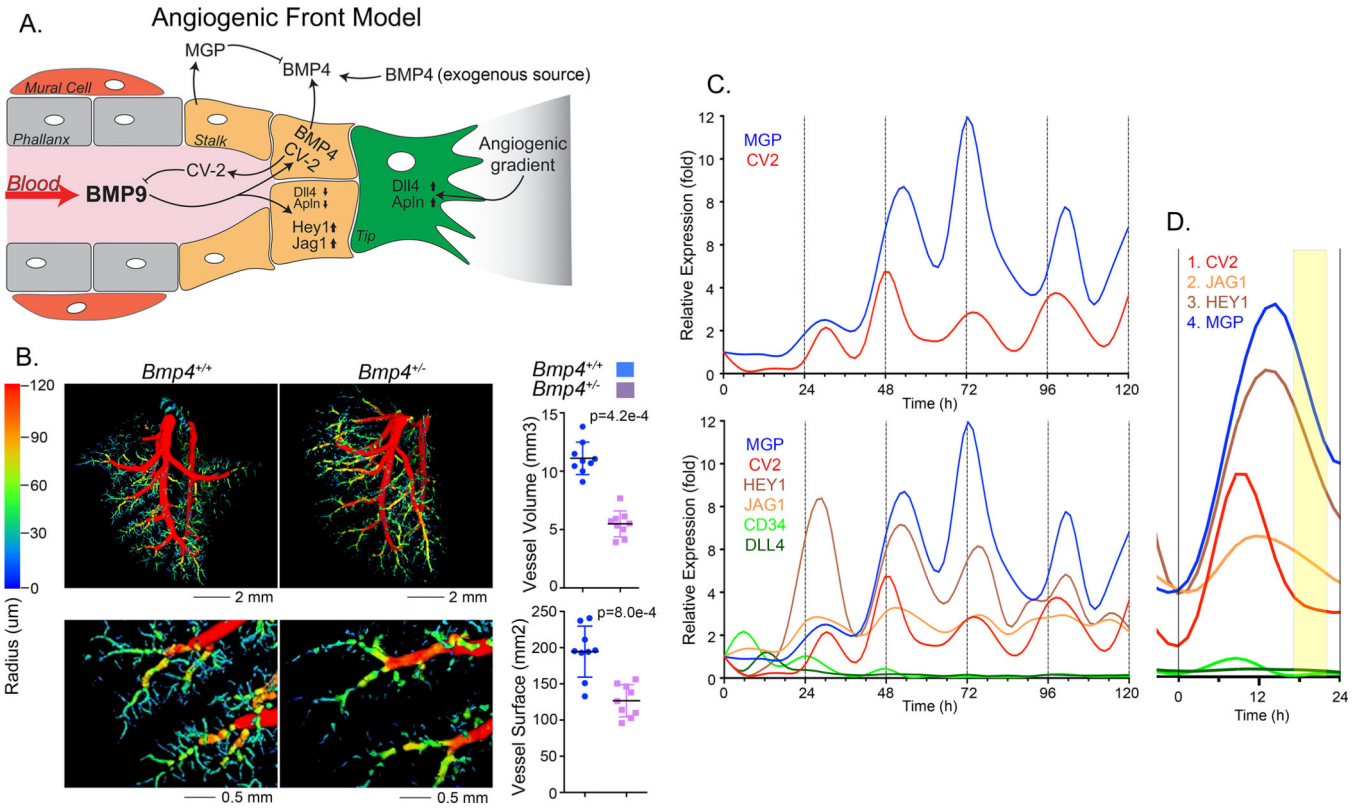

Figure 3: BMP9 triggers expression of stalk cell markers in HPAEC.

(A) Angiogenic front working model: BMP4 is available from exogenous sources or local ECs and induces expression of ALK1 and VEGF. The availability of ALK1 allows signaling by circulating BMP9. BMP9 induces CV2 and MGP that antagonizes BMP9 and BMP4, respectively, and coordinate the actions of the two BMPs. (B) Lung vasculature of mice wild type (*Bmp4*$^{+/+}$) mice and heterozygous for *Bmp4* gene deletion (*Bmp4*$^{+/-}$) mice by micro-CT imaging (left) with quantification of vessel surface and volume (right) (mean±SD; Mann-Whitney test, duplicate imaging). (C) Expression profiles for CV2, MGP, HEY1, JAG1, CD34 and DLL4 in HPAEC treated with BMP9 (10 ng/ml), RNA was collected every 6 hours for up to 120 hours, and expression was determined by qPCR, first normalized to GAPDH and then its own control. Adjusted R^2 and p-values from non-linear polynomial regression were as follows: *CV2*: adjusted R^2 0.328, p-value 0.025; *MGP*: adjusted R^2 0.594, p-value 0.001; *JAG1*: adjusted R^2 0.490, p-value 0.010; *HEY1*: adjusted R^2 0.339, p-value 0.022. Representative of 5 replicate experiments. (D) Enlarged view of the second oscillation in panel C.

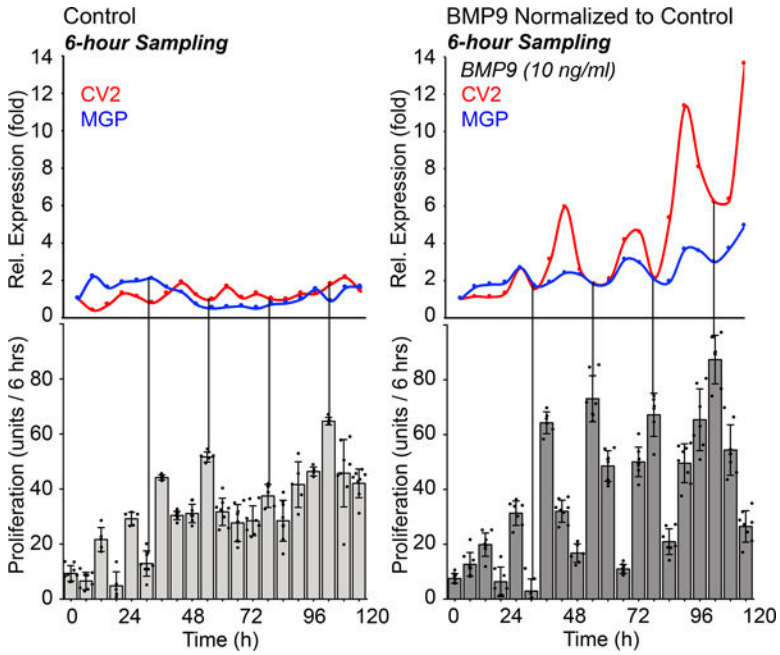

Figure 4: Proliferation in HPAECs in response to BMP9.

HPAECs were treated with control medium or BMP9 (10 ng/ml), RNA was collected every 6 hours for up to 120 hours, and expression of MGP was determined by qPCR and normalized to its own control. Each time point represents the mean of 3 determinations. Proliferation (change in cellular DNA content) was determined for each 6 hours period (mean±SD of ≥5 determinations; representative of 3 replicate experiments).

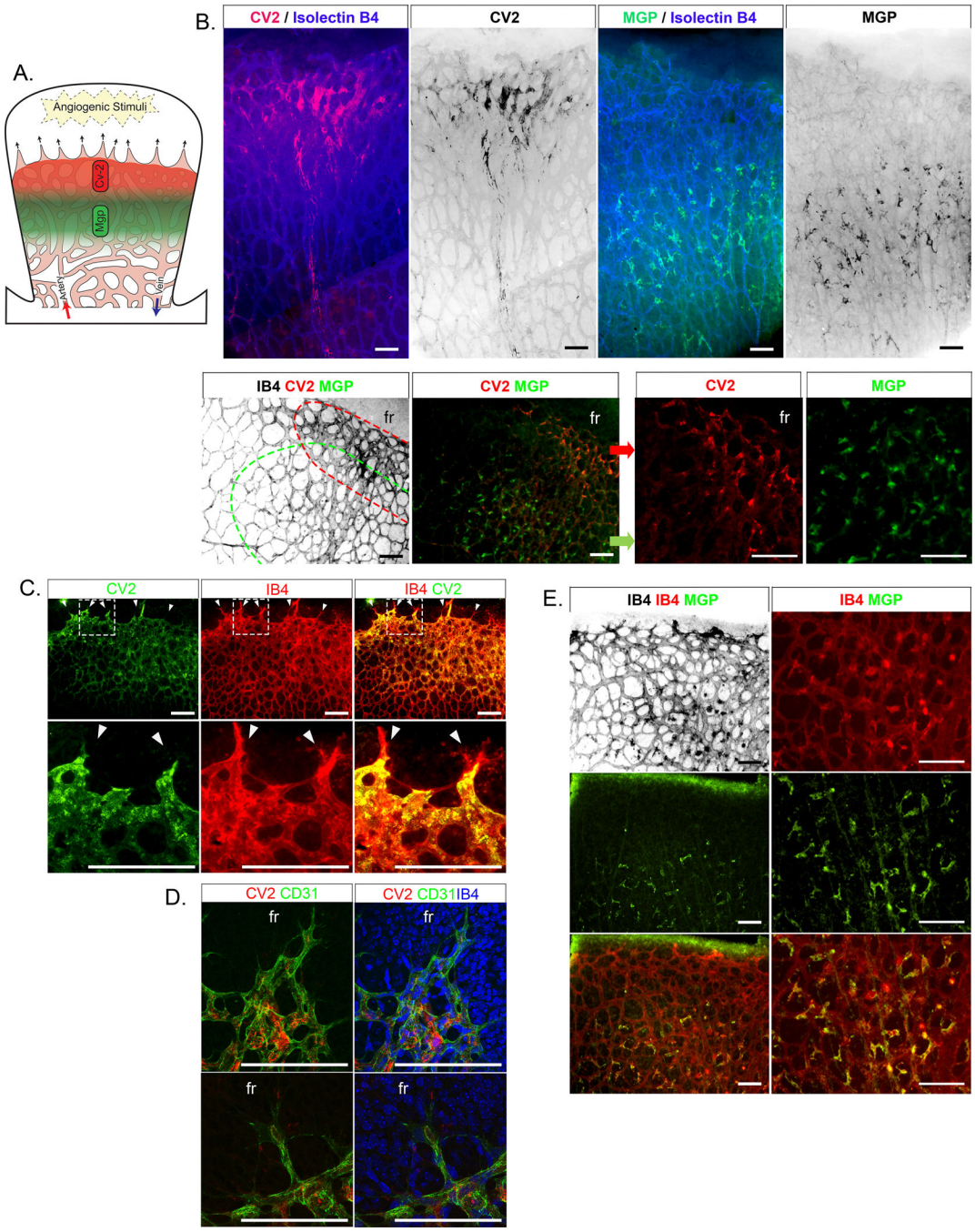

Figure 5: Distribution of CV2 and MGP in retinal angiogenesis (postnatal day 7, P7).

(A) Working model of growing retina with zones of CV2 and MGP. (B) (Left top) Immunofluorescence showing CV2 staining (red) together with Isolectin B4 (IB4) staining (blue) close to the retinal front (up) of mouse retinal vasculature; (Right top) MGP staining (green) together with IB4 staining (blue) away from the front. The bottom panels similarly show CV2 staining (red) and MGP staining (green) in two zones with CV2 closest to the front. (C) Close up of the vascular front; immunofluorescence showing CV2 staining (green) together with IB4 staining (red). No CV2 is detected in the tip cells (white arrows). (D)

Confocal microscopy showing CV2 staining (red) together with CD31 staining (green) in cells next to the tip cells. fr, front. (E) Immunofluorescence showing MGP staining (green) together with IB4 staining (red).

All bars, 200 μm; each panel is representative of ≥ 3 replicate experiments.

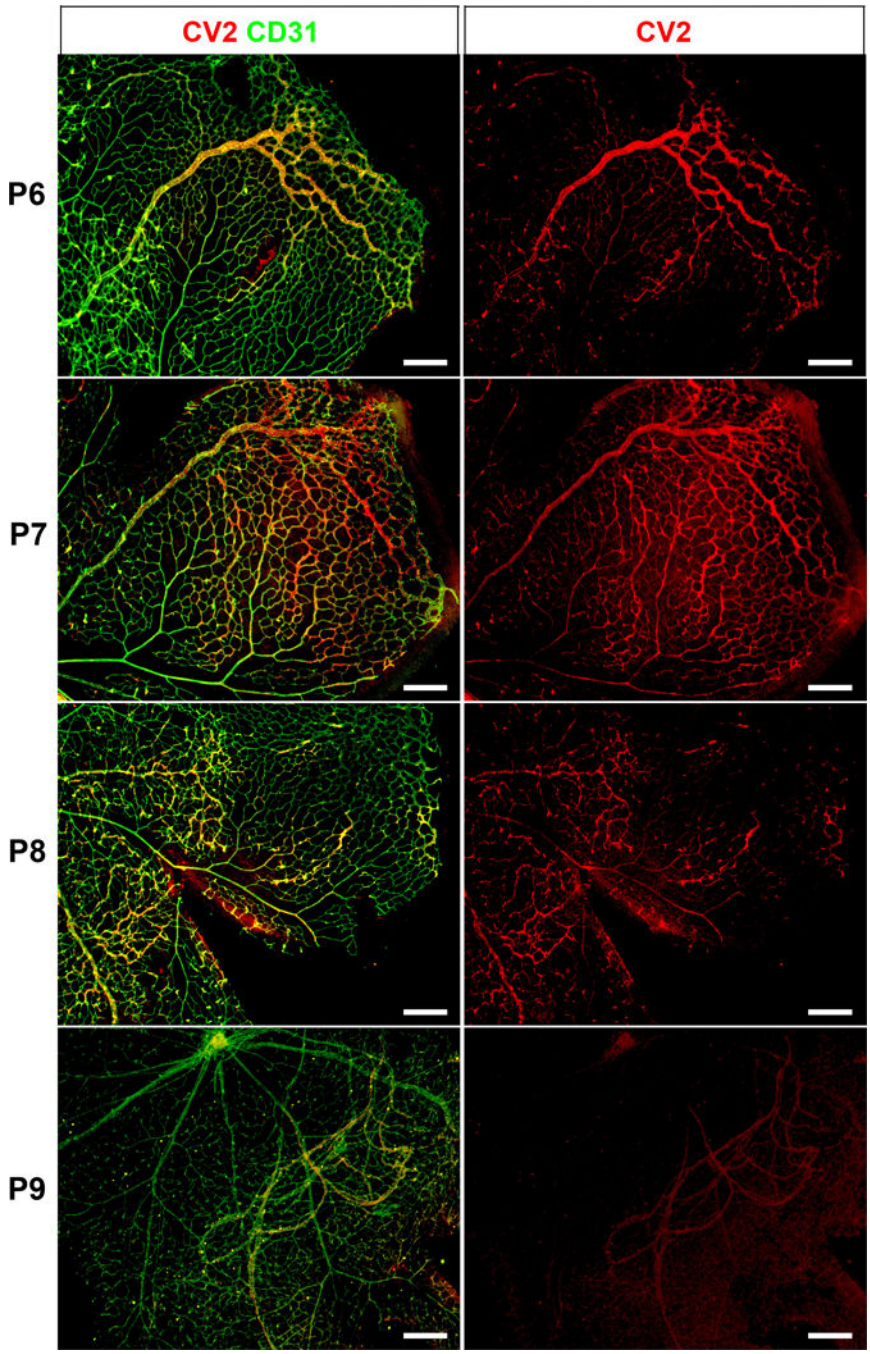

Figure 6: Distribution of CV2 in retinal angiogenesis (postnatal day 6–9).

Immunofluorescence showing CV2 (red) merged with CD31 (green) (left panels). The right panels show CV2 staining (red) alone. The location of the CV2 staining moves from the angiogenic front on P6 towards the middle of the retina, and disappears on P9. P, postnatal. All bars, 200 μm; each panel is representative of ≥ 3 replicate experiments.

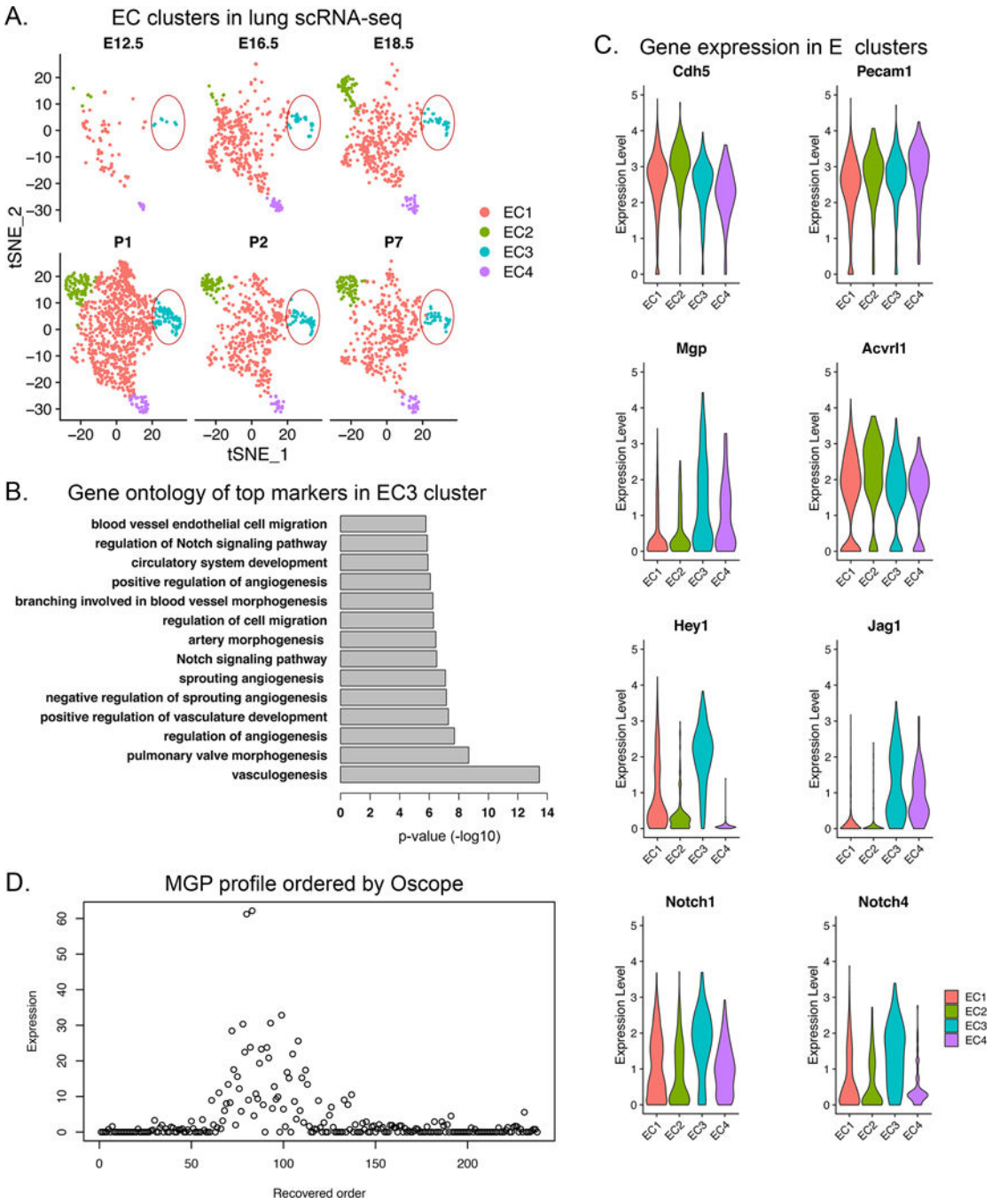

Figure 7: Angiogenic endothelial cell (EC) cluster in developing lungs.

(A) Pulmonary EC clusters were identified in the developing lungs from embryonic day (E)12.5 to postnatal day (P)7. EC cluster 3 (EC3) was detected at all time points (circled). (B) Gene ontology analysis of EC3 showed that the top markers in the EC3 cluster were classified under EC migration, regulation of Notch signaling, circulatory system development and angiogenesis. (C) Gene expression of ALK1, MGP, Hey1, Jag1, Notch1 and Notch 4 in the EC3 cluster. (D) MGP profile ordered by Oscope identified MGP as an oscillatory gene, suggesting that MGP is an important driver of repetitive cycles of growth.

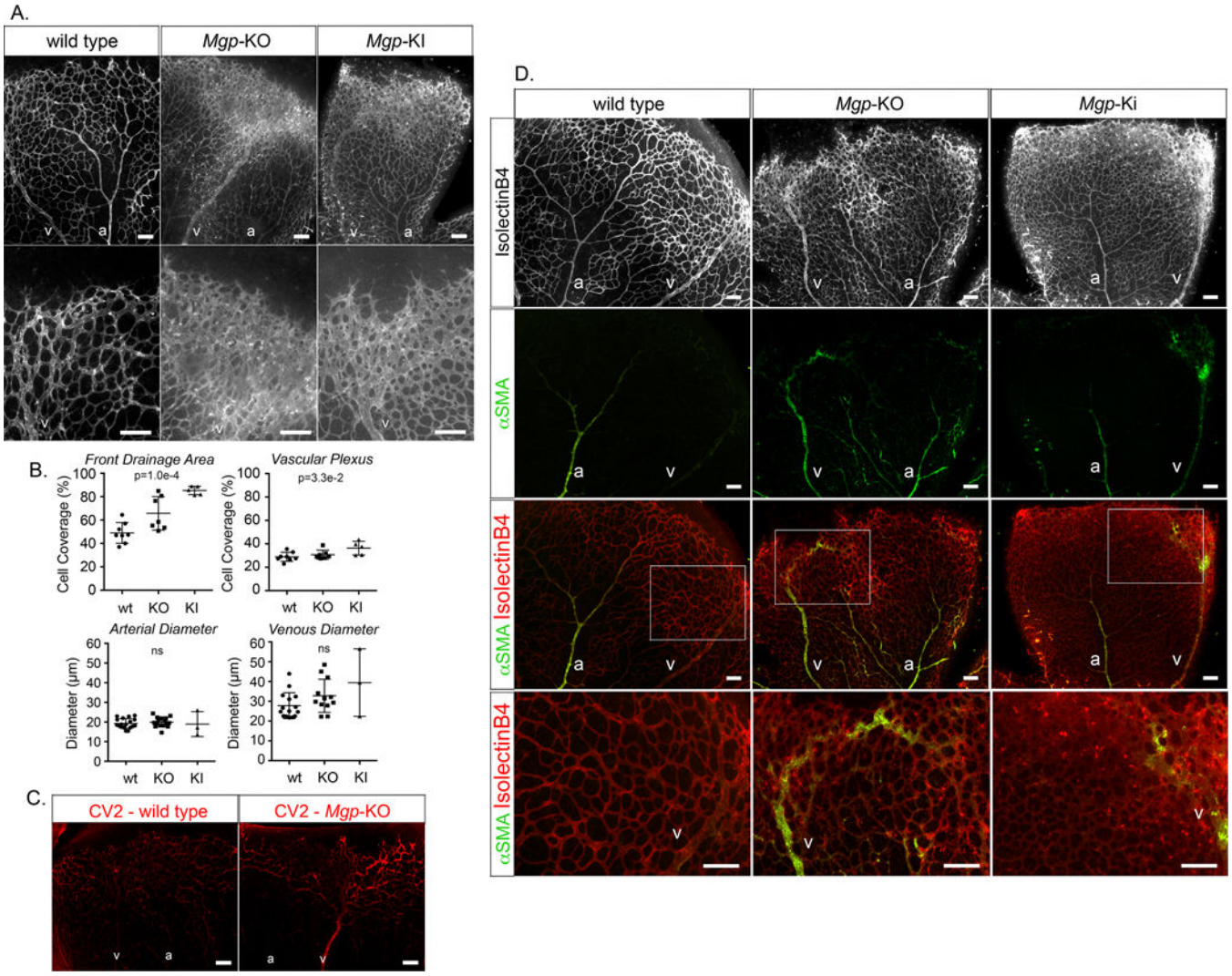

Figure 8: Effect of MGP deficiency on mouse retinal vasculature (postnatal day 7, P7).

(A) Mouse retinal vasculature from wild type, *Mgp*-knockout (KO) and *Mgp*-knockin (KI) mouse stained with Isolectin B4 (IB4) (white). (B) Quantitative analysis of percent cell coverage in the front drainage area and the vascular plexus (top) and arterial and venous diameters (bottom) (mean ± SD, determined from 8 or more retinas for wild type and *Mgp*-KO, and 3 or 5 retinas for *Mgp*-KI; Kruskal-Wallis test). (C) Immunofluorescence showing CV2 staining (red) in retina from wild type and *Mgp*-KO mouse. (D) (Top panels) mouse retinal vasculature from wild type, *Mgp*-KO and *Mgp*-KI mouse stained with Isolectin B4 (white). (Middle panels) alpha-smooth muscle actin (aSMA) staining (green) together with IB4 staining (red). (Bottom panels) Enlarged views of the indicated areas.

a; artery, v; vein; all bars, 200 µm; each panel is representative of ≥ 5 replicate staining experiments.